npj | precision oncology

Article

Published in partnership with The Hormel Institute, University of Minnesota

https://doi.org/10.1038/s41698-024-00748-x

Multi-omics analysis of Prolyl 3-hydroxylase 1 as a prognostic biomarker for immune infiltration in ccRCC

Guixin Ding[1,3], Tianqi Wang[1,3], Fengze Sun[1,3], Ming Liu[1], Gonglin Tang[1], Shengqiang Yu[1], Yongli Chu[1,2], Jian Ma[1], Yuanshan Cui[1] ✉, Gang Wu[1] ✉ & Jitao Wu[1] ✉

The formation of human collagen requires the presence of Prolyl 3-hydroxylase 1 (P3H1), but the regulatory mechanism of P3H1 remained insufficiently understood. Our study aimed to identify the role of P3H1 in clear cell renal cell carcinoma (ccRCC). P3H1 expression in ccRCC was validated using multiple databases and in vitro experiments. We performed a correlation analysis of P3H1 with drug sensitivity, immune checkpoints, and immune cell infiltration using transcriptome and single-cell sequencing. Drawing upon the Encyclopedia of RNA Interactomes database, we selected P3H1 as the focal point of our investigation, meticulously uncovering the intricate network of microRNAs and lncRNAs that potentially orchestrate ceRNA mechanisms. This study employs a multidimensional approach integrating vitro assays and multi-omics bioinformatics analyses to investigate P3H1's impact on ccRCC prognosis, immune modulation, immune checkpoints, ceRNA regulatory network, drug sensitivity, and therapeutic responses, aiming to uncover new insights into its therapeutic potential and inform future clinical strategies.

Renal cell carcinoma (RCC) encompasses multiple subtypes, with clear cell renal cell carcinoma (ccRCC) being the most prevalent, accounting for 75-80% of all pathological types[1,2]. Despite early surgical intervention, approximately 30% of ccRCC patients eventually experience relapse and develop metastases[3]. ccRCC poses a significant therapeutic challenge due to its inherent resistance to chemotherapy and radiotherapy. Poor prognosis is typically associated with advanced or metastatic renal cancer, with the five-year survival rate for stage IV ccRCC patients being less than 20%[4]. Immunotherapy with checkpoint inhibitors has emerged as a promising strategy for improving survival outcomes in ccRCC[5,6]. Although numerous potential genes have been proposed as prognostic markers for ccRCC, only a few have been validated as effective targets for diagnosis or treatment[7,8]. Therefore, there is an urgent need to thoroughly understand the molecular processes underlying ccRCC and to develop effective diagnostic and treatment strategies.

Prolyl 3-hydroxylase 1 (P3H1), also known as leucine proline-enriched proteoglycan 1 (LEPRE1), is a growth inhibitor and a member of the prolyl 3-hydroxylase family[9]. P3H1 plays a critical role in collagen assembly, folding, synthesis, and proline hydroxylation, making it an essential protein for these processes[10,11]. Furthermore, P3H1 is known to regulate intracellular signaling and matrix interactions[12], and it is involved in the invasion, migration, and proliferation of osteosarcoma cell lines[13]. Elevated expression levels of P3H1 have been observed in different types of solid tumors, such as colorectal, lung, and breast cancer[14–16]. Studies show that the P3H1 gene is closely related to immune infiltration in tumors[17,18]. Whereas the oncogenicity, immune infiltration, and clinical significance of P3H1 in ccRCC remain uncertain.

In this study, we employed multiple methods to evaluate the expression of P3H1 in ccRCC and validated the results through immunohistochemistry (IHC) and in vitro experiments. We aimed to investigate the potential association between P3H1 expression and prognosis in ccRCC patients with diverse clinical-pathological features, as well as the immunotherapeutic and chemotherapeutic response of P3H1 in ccRCC. To explore the potential involvement of P3H1 in ccRCC, we performed functional enrichment analysis. Moreover, leveraging cutting-edge tools like ESTIMATE, TIMER, EPIC, and CIBERSORT, we explored the intricate interplay between P3H1 expression and immune cell infiltration within the ccRCC microenvironment. This exploration not only enhances our understanding of tumor-immune interactions but also identifies opportunities for immunotherapeutic strategies tailored to ccRCC patients based on their P3H1 expression profiles. Furthermore, our comprehensive analysis of immune checkpoints, integrating data from the TCGA cohort without immunotherapy and the

[1]Department of Urology, Yantai Yuhuangding Hospital, Qingdao University, Yantai, Shandong, China. [2]Department of Scientific Research, Yantai Yuhuangding Hospital, Qingdao University, Yantai, Shandong, China. [3]These authors contributed equally: Guixin Ding, Tianqi Wang, Fengze Sun. ✉e-mail: doctorcuiys@163.com; wugd1209@163.com; wjturology@163.com

CheckMate 025 cohort with immunotherapy, elucidated numerous correlations between immune checkpoint genes and P3H1. Long noncoding RNAs (lncRNAs) and circular RNAs (circRNA) can bind to microRNAs (miRNAs) in the cell and act as a sponge, thereby modulating the protein expression of messenger RNA (mRNA)[19,20]. This has led to the suggestion of a theory called "competing endogenous RNA (ceRNA)"[21–23]. By adopting the ceRNA mechanism, we explored the potential involvement of lncRNAs and miRNAs in P3H1 regulation and prepared for subsequent basic research. This study employs a multidimensional approach integrating into vitro assays and multi-omics bioinformatics analyses to investigate P3H1's impact on ccRCC prognosis, immune modulation, immune checkpoints, ceRNA regulatory network, drug sensitivity, and therapeutic responses, aiming to uncover new insights into its therapeutic potential and inform future clinical strategies.

Methods

The Human Protein Atlas (HPA) and the Harmonizome database

The HPA database (https://www.proteinatlas.org), developed through the integration of proteomics, transcriptomics, and systems biology, offers a comprehensive resource for investigating protein expression and immunohistochemistry in both tumor and normal tissues[24]. Within this invaluable resource, we extracted the P3H1 RNA expression summary. Furthermore, we explored the expression patterns of P3H1 in diverse immune cells within the plasma, utilizing the Schmiedel dataset and Monaco scaled dataset available in the HPA. For additional insights into P3H1 expression, the Harmonizome database (https://maayanlab.cloud/Harmonizome/) provided comprehensive information regarding its expression in various tissues and cell lines.

Immune checkpoint blockade (ICB) cohort

CheckMate 025 (CM-025) is a randomized Phase III trial of Nivolumab (anti-PD-1) for ccRCC treatment[25]. The study provided RNA sequencing (RNA-seq) data from tumor specimens of 181 ccRCC patients receiving anti-PD-1 therapy. We obtained both clinical and RNA-seq data for these patients from the supplemental materials of this study[25].

mRNA and protein expression of P3H1 in ccRCC

The present study utilized several publicly available databases to collect data for analysis. The Cancer Genome Atlas (TCGA) database (https://portal.gdc.cancer.gov/) contains 33 cancer types with genomic, transcriptomic, proteomic, and clinical information. We explored the TCGA database to obtain the original RNA expression data of KIRC patients, which included 72 normal tissues and 539 tumor samples. Additionally, we accessed the GEO database (https://www.ncbi.nlm.nih.gov/geo/), which provides gene expression data submitted by research institutions globally. The microarray dataset GSE53757, consisting of 72 normal tissue samples and 72 tumor tissues and using the GPL570 sequencing platform was downloaded from the GEO database for analysis.

The UALCAN database (http://ualcan.path.uab.edu/index.html) provides an interactive and user-friendly platform for analyzing cancer transcriptomes, featuring published data from TCGA and MET500. P3H1 protein expression levels were analyzed using UALCAN, which sourced the data from CPTAC (Clinical Proteomic Tumor Analysis Consortium).

Informed consent procedure

The study was conducted in accordance with the Declaration of Helsinki, and written informed consent was obtained from all patients prior to participation. All experimental procedures were approved by the ethics committee of Yantai Yuhuangding Hospital, Qingdao University.

Cell lines and cell culture

The ccRCC cell lines (786-O, 769-P, Caki-2, ACHN, A498) and the renal tubular epithelial cell line (HK-2) were obtained from the Cell Bank of the Chinese Academy of Sciences. The ccRCC cell lines were cultured in RPMI1640 (BI, Israel), while HK-2 cells were cultured in DMEM (BI, Israel). All media used in the experiment were supplemented with 10% fetal bovine serum (FBS) and 1% penicillin and streptomycin. Each cell type was cultured in a humidified incubator set at 37 °C and 5% carbon dioxide with optimal conditions.

Sample collection

We obtained 13 cases of ccRCC tissues and adjacent normal tissues from the Department of Urology at Yantai Yuhuangding Hospital, Qingdao University. All tissue samples were immediately flash-frozen in liquid nitrogen after resection and then stored at −80 °C for subsequent qRT-PCR analysis. Additionally, 20 paraffin-embedded archived ccRCC samples were obtained from our hospital for immunohistochemistry (IHC) analysis. These ccRCC samples were from patients who underwent either partial nephrectomy or radical nephrectomy. The pathological specimens were carefully examined and verified by two independent pathologists to ensure accuracy and consistency.

RNA extraction and quantitative reverse transcriptase polymerase chain reaction (qRT-PCR)

Total RNA was extracted from the samples using Trizol reagent (Pufei, Shanghai, China) following the manufacturer's instructions. RNA quantification was performed at 260 nm using a spectrophotometer (Thermo Fisher, USA). The extracted RNA was then reverse-transcribed into complementary DNA (cDNA) using the Promega M-MLV kit (Accurate Biology, China). qRT-PCR was performed on a fluorescent quantitative PCR instrument (Thermo Fisher, USA) to determine the mRNA level of the gene of interest based on the SYBR green fluorescence level. The $2^{-\Delta\Delta CT}$ method, using GAPDH as a control, was employed to evaluate the relative expression levels of the target mRNAs. The primer sequences used for qRT-PCR were provided in Supplemental Table 1.

Western blot

The protein lysates were loaded into individual lanes and subjected to analysis by 10% sodium dodecyl sulfate-polyacrylamide gel electrophoresis (SDS-PAGE). Subsequently, the separated proteins were transferred onto nitrocellulose (NC) membranes (Millipore, Darmstadt, Germany) for further analysis. After blocking the membrane with a 5% non-fat milk solution in Tris-buffered saline with Tween for 1 hour, the membrane was incubated with rabbit polyclonal primary antibodies against P3H1 (Proteintech, China) at a dilution of 1:1000. The incubation was carried out overnight at 4 °C. Following three 10-minute rinses with TBST, the membrane was incubated at room temperature for 1 hour with HRP-conjugated secondary antibodies (1:5000) (Santa Cruz, CA, USA). Immunoreactive bands were detected using a chemiluminescent detection system (ECL, Pierce, Rockford, IL, USA). The quantification of protein levels was conducted by referencing the β-actin protein as a basis for calculation.

Immunohistochemical staining

All tumor sections were subjected to routine dewaxing and rehydration methods. Subsequently, the sections were incubated in 3% H_2O_2 for 30 minutes to block endogenous peroxidase activity. The slides were then incubated with rabbit polyclonal primary antibodies against P3H1 at a dilution of 1:100 in a humidified chamber overnight at 4 °C. The sections underwent staining using 3,3'-diaminobenzidine (DAB) and were subsequently counterstained with hematoxylin following the manufacturer's instructions. The percentage of P3H1 immune-positive tumor cells was used to assign a score, with a score of four when ≥50% of cells were positive, three when 26-50%, two when 6-25%, and one when ≤5%. The staining intensity was scored as 3 (strong), 2 (moderate), 1 (weak), or 0 (negative). The two scores were multiplied, and the resulting score was utilized to categorize P3H1 expression as either high (>6) or low (≤6).

P3H1 immune correlation analysis

Multiple R packages, including "ggplot2," "corrplot," "limma," "ggExtra," "vioplot," "ggpubr," "reshape2," and "GSVA," were applied to visualize the

association between P3H1 and various immune cells and immune checkpoints. ESTIMATE[26], TIMER[27,28], EPIC[29], and CIBERSORT[30] computational algorithms were used to compute the abundance of tumor-infiltrating immune cells in ccRCC specimens from TCGA. The relationship between immune checkpoints (PDCD1, PDCD1LG2, CD274, CTLA4, TIGIT, HAVCR2, and LAG3) and P3H1 was analyzed using the GEPIA2 database (http://gepia2.cancer-pku.cn/#index)[31], the TIMER 2.0 database (http://timer.cistrome.org/)[27], and the CheckMate 025 (CM-025) cohort ($N = 181$)[25].

Tumor-immune system interaction database

TISIDB, an integrated repository tool available at (http://cis.hku.hk/TISIDB), endeavors to unravel the intricate interplay between the immune system and tumors[32]. Leveraging the database, we assessed the intricate association between P3H1 and the expression patterns of chemokines/chemokine receptors, as well as immunoinhibitors/immunostimulators.

P3H1 expression in the tumor microenvironment

To obtain a comprehensive understanding of the tumor microenvironment (TME) at a single-cell level, we utilized the scRNA-seq database called Tumor Immune Single-cell Hub 2 (TISCH2)[33], which can be accessed at http://tisch.comp-genomics.org/. In this investigation, we delved into the expression patterns of P3H1 within the TME of ccRCC, leveraging the invaluable resources provided by this database.

STRINGS analysis

We utilized the STRINGS online analysis website (http://www.string-db.org) to conduct a protein-protein interaction (PPI) network analysis on P3H1[34]. The PPI network was created with the following parameters: 1) Active interaction sources including Co-expression, Databases, Experiments, and Textmining; 2) Network edge meaning determined based on available evidence; 3) Minimum required interaction score set to high confidence (0.400); 4) Maximum number of interactions allowed set to 20.

Function enrichment analysis

The functional enrichment analysis categorizes gene lists based on their functions and correlations with biological characteristics. We performed Kyoto Encyclopedia of Genes and Genomes (KEGG) and Gene Ontology (GO) analysis on P3H1 and the 20 co-expressed genes using the clusterProfiler package[35]. The aim was to gain insight into biological processes, cellular components, molecular functions, and significant signaling pathways. The analysis data were visualized using the ggplot2 software package.

Kaplan–Meier plotter database

The Kaplan-Meier plotter (http://kmplot.com/analysis/), a tool for prognostic analysis, includes data on 54,675 genes from 10,461 cancer samples to predict survival. To evaluate the prognostic significance of P3H1 expression in relevant immune cell subgroups, we conducted a log-rank p-value analysis and calculated the hazard ratios (HR) with 95% confidence intervals (CI).

Analysis of clinical prognostic factors

We utilized the "ggpubr" and "limma" packages to assess and visualize the correlation between each prognostic factor and P3H1 expression. We employed the "rms," "regplot," "timeROC," "survminer," and "survival" packages to generate nomograms, calibration curves, and receiver operating characteristic (ROC) curves. Multivariate and univariate Cox analyses were performed using the "survival" package.

Establishment of mRNA-miRNA-lncRNA co-expression network

Data on mRNA-miRNA and miRNA-lncRNA interactions were obtained from the Starbase database (http://starbase.sysu.edu.cn/)[36]. A program number ≥ 1 was set as the screening criterion for mRNA-miRNA interactions. The R package was used to screen correlation coefficient values, survival curve values, and differential expression values. A negative correlation between expression levels was defined as $r < -0.1$, and a positive correlation was defined as $r > 0.1$. The significant threshold for differential expression was set at $P < 0.01$, and for survival curves, it was set at $P < 0.05$. We utilized the R language package to plot the data and construct a crucial lncRNA-miRNA-mRNA ceRNA network for ccRCC. The potential ceRNA mechanisms associated with P3H1 were illustrated using BioRender.

P3H1-related drug sensitivity evaluation

The determination of the half maximal inhibitory concentration (IC50), which represents the concentration required to inhibit drug activity by 50%, was carried out using the 'pRRophetic' package[37] along with its dependencies, including "genefilter," "sva," "ridge," "preprocessCore," and "car." These packages provide information about the effects of various drugs.

Statistical analysis

Statistical analysis was conducted using GraphPad Prism and SPSS software. The data are presented as the mean ± standard error from a minimum of three experiments. The Mann-Whitney U test and paired t-test were performed to determine differences between ccRCC and paired normal tissues. The Wilcoxon test was employed for pairwise comparisons between two groups, while the Kruskal-Wallis test was used for comparisons across multiple groups. Kaplan-Meier curves were utilized to analyze the expression level of P3H1 and its prognostic significance in ccRCC patients. Time dependence ROC curves of P3H1 expression were used to evaluate the predictive efficiency of P3H1 in ccRCC. A significance level of $P < 0.05$ was considered for all analyses. The flow chart of the study is presented in Fig. 1.

Results

Expression landscape and expression pattern of P3H1 in pan-cancer perspective

As shown in Fig. 2A, P3H1 is widely expressed across various tissues and organs. The consensus dataset revealed that P3H1 mRNA was predominantly expressed in the duodenum and placenta (Fig. 2B). UMAP plots indicated that P3H1 expression was observed in erythroid cells, skeletal myocytes, Müller glial cells, and squamous epithelial cells (Fig. 2C). Figure 2D and E illustrate the details of P3H1 mRNA expression across different tissues and cell types.

Aberrant P3H1 expression in ccRCC

To determine the differences in P3H1 expression between tumors and normal tissues, we analyzed the mRNA levels of P3H1 using the TIMER database (Fig. 3A) and the TCGA database (Fig. 3B) across various cancer types. This analysis revealed that most cancer types, including bladder urothelial carcinoma (BLCA), breast invasive carcinoma (BRCA), cholangiocarcinoma (CHOL), colon adenocarcinoma (COAD), esophageal carcinoma (ESCA), glioblastoma multiforme (GBM), head and neck squamous cell carcinoma (HNSC), kidney renal clear cell carcinoma (KIRC), kidney renal papillary cell carcinoma (KIRP), liver hepatocellular carcinoma (LIHC), lung adenocarcinoma (LUAD), lung squamous cell carcinoma (LUSC), prostate adenocarcinoma (PRAD), rectum adenocarcinoma (READ), stomach adenocarcinoma (STAD), thyroid carcinoma (THCA), and uterine corpus endometrial carcinoma (UCEC), exhibited higher expression compared to normal tissues (Fig. 3A, B). Conversely, kidney chromophobe (KICH) exhibited lower expression levels of P3H1 (Fig. 3A, B). To determine the mRNA and protein expression of P3H1 in ccRCC, we analyzed the expression profile from TCGA, GEO, HPA, and UALCAD datasets. Data from the TCGA and GEO databases revealed that P3H1 was significantly differentially expressed in malignant tumors ($P < 0.001$; Fig. 3C–E). We were able to conduct an analysis of P3H1 protein expression by the CPTAC and HPA database. Our findings indicated a significant increase in P3H1 protein expression in ccRCC when compared to paracancer tissue (Fig. 3F–H). Additionally, the validation of protein expression was conducted using immunohistochemical staining, which

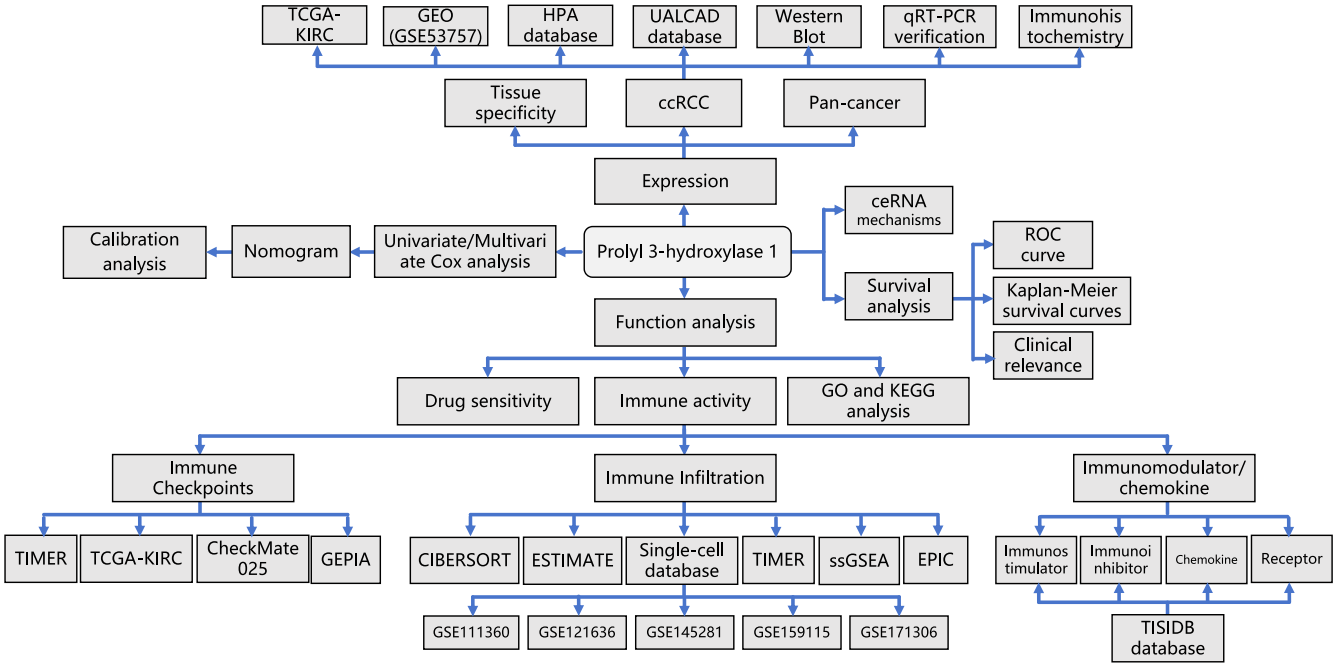

Fig. 1 | Flowchart.

shows that P3H1 protein expression was elevated and highly expressed in cancer tissues (Fig. 3I–L). Furthermore, qRT-PCR was performed to examine the expression of P3H1 in 13 pairs of ccRCC cases and adjacent normal tissues (Fig. 3M). We also verified that P3H1 expression was higher in several ccRCC cell lines (786-O, 769-P, CAKI-2, ACHN, and A498) compared to the control cell line (HK-2) using qRT-PCR and WB (Fig. 3N, O). In conclusion, multiple databases and experiments jointly verified that the expression level of P3H1 mRNA and protein in ccRCC was significantly higher than that in normal renal tissue.

Relationships between P3H1 mRNA levels and clinical pathological features of ccRCC patients

Baseline characteristics of patients with ccRCC, as accessed from the TCGA database are presented in Supplemental Table 2. As depicted in Fig. 4D–L, elevated expression of P3H1 was significantly correlated with various clinical features including T stage ($P < 0.001$), M stage ($P < 0.05$), histological grade ($P < 0.001$), pathological stage ($P < 0.001$), primary therapy outcome ($P < 0.001$), overall survival (OS) event ($P < 0.001$), disease-specific survival (DSS) event ($P < 0.001$) and progression-free interval (PFI) event ($P < 0.001$). However, there was no statistically significant association between P3H1 expression and other clinicopathological features, such as age, gender, laterality, and N stage (Fig. 4A–C and E). These results suggest that high P3H1 expression may be associated with tumor progression and poorer prognosis in patients with ccRCC.

Value of P3H1 expression in diagnosis and predicting prognosis

We conducted the following analyses to further explore the prognostic and diagnostic significance of P3H1 in ccRCC. In this study, we continued to explore the potential relationship between P3H1 expression and the prognosis of ccRCC patients. Kaplan-Meier curves were employed to examine the correlation between P3H1 mRNA expression and OS, DSS, and PFI in ccRCC patients. Figure 4M–O indicated that high P3H1 expression is significantly associated with shorter OS, DSS, and PFI in ccRCC patients, with hazard ratios (HR) of 2.48 (1.80–3.40) for OS ($P < 0.001$), 3.71 (2.40-5.73) for DSS ($P < 0.001$), and 3.16 (2.25–4.45) for PFI ($P < 0.001$).

The predictive performance of P3H1 for OS in ccRCC patients was evaluated using time-dependent receiver operating characteristic (ROC) analysis. The area under the curve (AUC) was calculated for 1, 3, and 5 years, yielding values of 0.709, 0.659, and 0.682, respectively (Fig. 4P). These results indicate that P3H1 has a strong predictive capacity for OS over five years. Additionally, the time-dependent ROC curves for DSS and PFI also demonstrated strong predictive capacity over five years (Fig. 4Q, R). The ROC curve analysis for diagnosis showed that P3H1 expression accurately distinguished tumors from normal tissues, with an AUC of 0.939 (Fig. 4S). Multivariate Cox regression analysis identified P3H1 expression (HR, 1.951; 95% CI: 1.404–2.712; $P < 0.001$), age (HR, 1.625; 95% CI: 1.191–2.218; $P = 0.002$), pathologic stage (HR, 2.645; 95% CI: 1.875–3.733; $P < 0.001$), and histologic grade (HR, 1.753; 95% CI: 1.219–2.520; $P = 0.002$) as independent risk factors for survival prognosis in ccRCC (Supplemental Table 3). The nomogram model presented in Fig. 4T combines the independent prognostic factors identified in the multivariate analysis, including age, pathologic grade, and histologic grade. A nomogram model was built, which can be used to predict the survival probabilities at 1-, 3-, and 5-years for patients in clinical practice (Fig. 4T). The calibration plots show that the predicted probabilities from the nomogram model align well with the observed probabilities, as the bias-corrected line closely follows the ideal 45-degree line (Fig. 4U–W). Overall, these findings suggest that P3H1 may serve as a valuable biomarker for both diagnosing and predicting the prognosis of ccRCC patients.

DEGs analysis

DEG analysis between the high- and low-P3H1 groups in the TCGA cohort revealed 2346 up-regulated and 1261 down-regulated DEGs that were statistically significant (p.adj < 0.05, $|\log2(FC)| > 1$) (Supplemental Fig. 1A). The heatmap displayed the top fifty significant up- and-down-regulated genes (Supplemental Fig. 1B).

P3H1-related functional enrichment analysis in ccRCC

The OPEN TARGET platform revealed the involvement of P3H1 in various disorders (Fig. 5A). A PPI network was constructed in "Cytoscape" based on P3H1 and its 20 co-expressed genes from the STRING database (Fig. 5B). GO and KEGG pathway enrichment analyses were conducted on the top 20 correlated genes of P3H1 to investigate the potential functions of P3H1 in ccRCC (Fig. 5C–F). Correlation analysis showed that P3H1 was positively correlated with its co-expressed genes (Fig. 5G).The KEGG pathway enrichment analysis revealed that P3H1 was associated with several pathways, including "protein digestion and absorption," "ECM-receptor

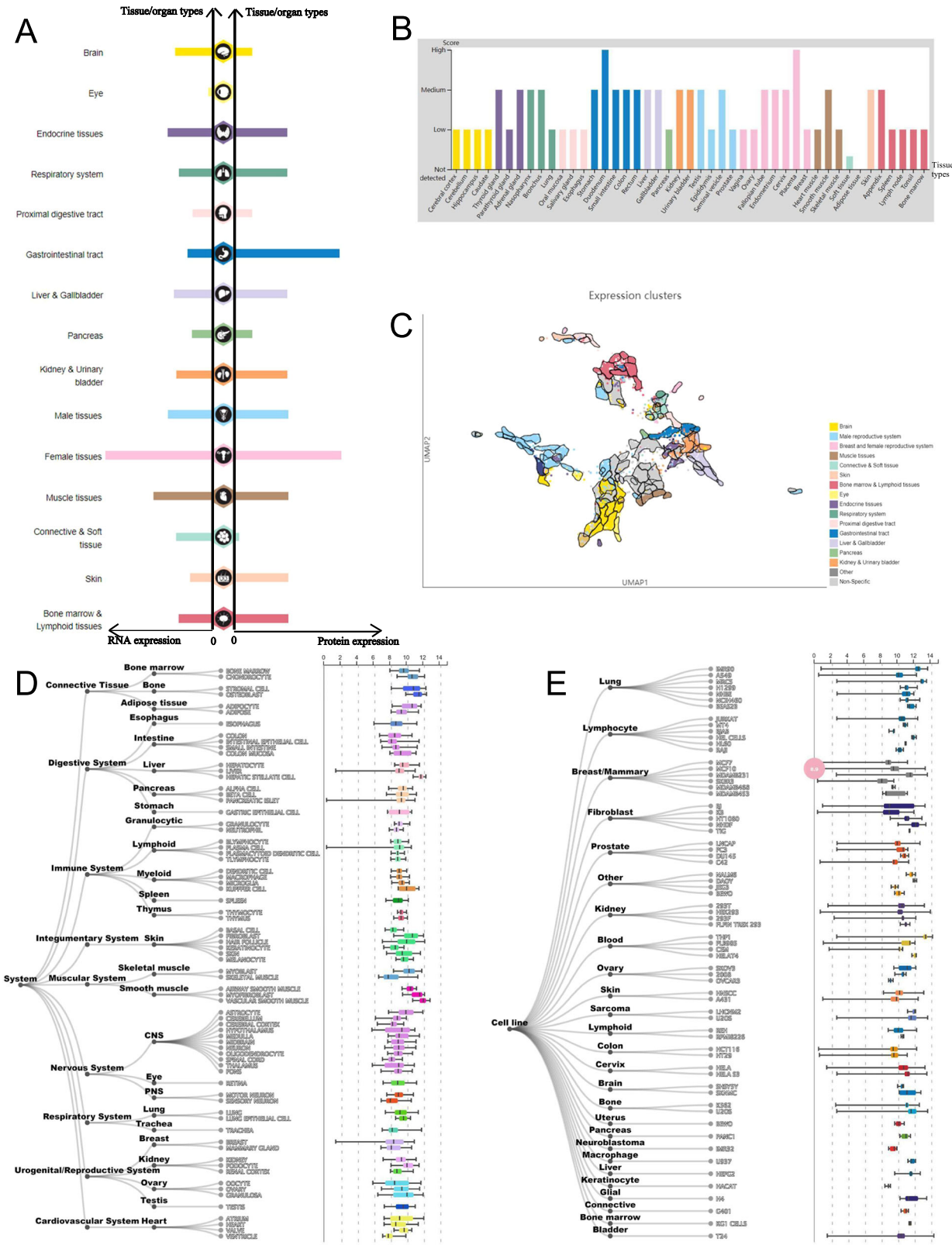

Fig. 2 | RNA and protein expression profile of P3H1 in human organs and tissues. **A** The summary of the mRNA and protein expression of P3H1 in human organs and tissues; **B** P3H1 mRNA expression summary in different human organs and tissues based on consensus dataset; **C** The interactive UMAP plot displays the gene clusters resulting from Louvain clustering of gene expression across all single cell types; **D**, **E** Details of P3H1 mRNA expression in different tissues and cell lines.

interaction," "AGE-RAGE signaling pathway in diabetic complication," "Relaxin signaling pathway," and "PI3K-Akt signaling pathway" (Fig. 5F). The GO enrichment analysis indicated that P3H1 is involved in "extracellular structure organization" (BP, GO:0043062), "endoplasmic reticulum lumen" (CC, GO:0005788), and "extracellular matrix structural constituent" (MF, GO:0030020) (Fig. 5C–E). These results suggest that P3H1 plays a crucial role in multiple signaling pathways and both intracellular and extracellular functions, contributing significantly to the onset and progression of ccRCC.

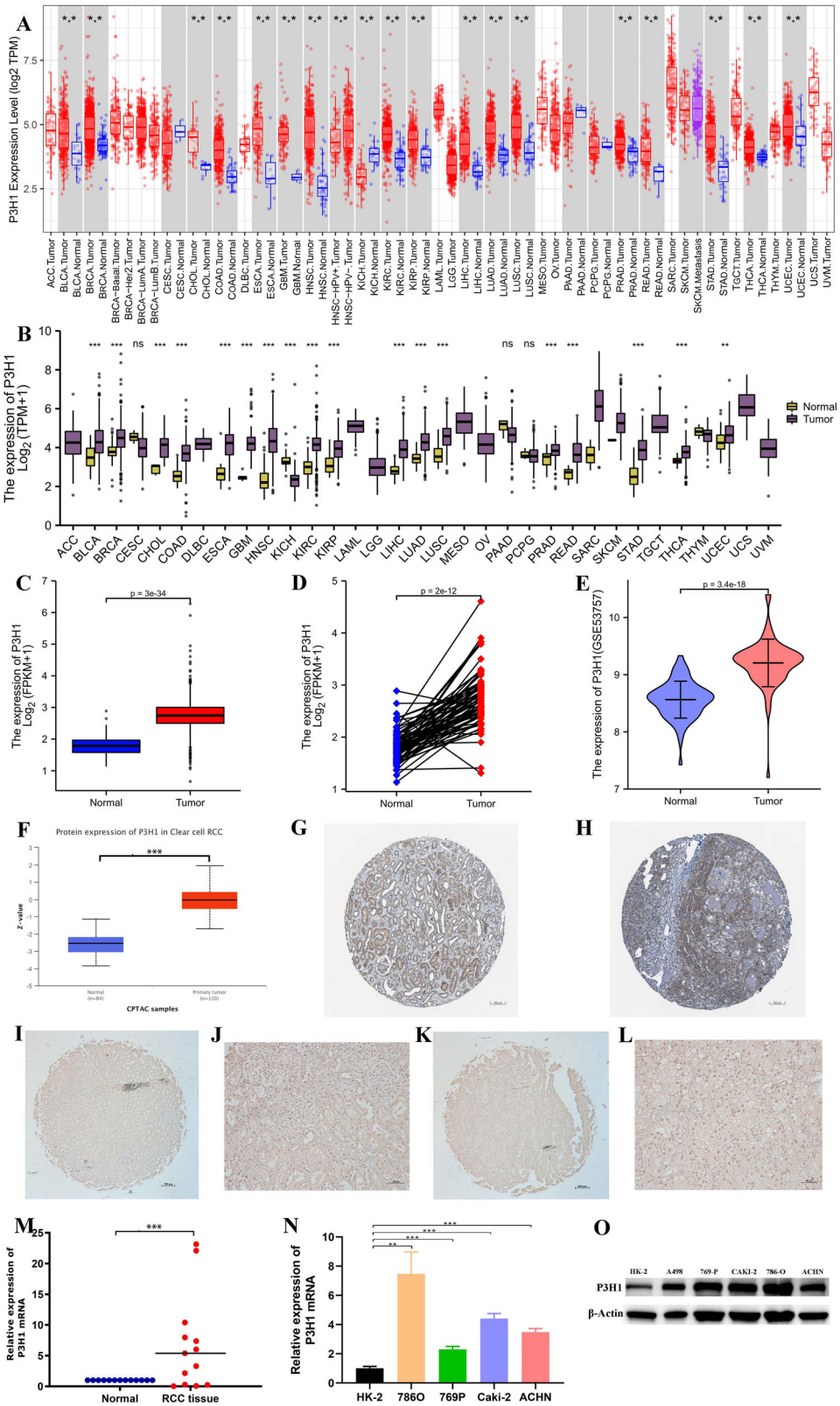

Fig. 3 | The expression of P3H1 in ccRCC and pan-carcinoma. A P3H1 expression levels in different tumor types were measured using the TIMER2.0 database. **B** TCGA database analysis shows the P3H1 expression levels in 33 types of cancer tissues and their corresponding adjacent normal tissues. **C** The mRNA expression level of P3H1 in 539 ccRCC samples and 72 normal samples. **D** The mRNA expression level of P3H1 in 72 ccRCC and matched-adjacent normal samples. **E** The mRNA expression level of P3H1 in tumor samples matched in GEO database was higher than that in adjacent normal samples ($P < 0.001$). **F** Protein expression level of P3H1 based on the CPTAC database. **G** Normal tissues: the protein levels of P3H1 based on the Human Protein Atlas. **H** Tumor tissues: the protein levels of P3H1 based on the Human Protein Atlas. **I**, **J** Normal renal tissue. **K**, **L** ccRCC tissue. **M** qRT-PCR experiment on matched samples of 13 eligible ccRCC patients. qRT-PCR **N** and WB **O** experiments to verify the expression of P3H1 gene in renal cell carcinoma cell lines.

Correlation between immune infiltration and expression of P3H1 in ccRCC

We utilized multiple immune algorithms (ESTIMATE, TIMER, EPIC, and CIBERSORT) to examine immune cell infiltration in ccRCC patients, categorizing 503 tumor transcriptome sequencing samples from TCGA-KIRC into high and low P3H1 expression groups based on average P3H1 levels, to investigate the correlation between P3H1 expression and immune infiltration. The ESTIMATE algorithm revealed high P3H1 expression patients had significantly higher immune scores ($P < 0.001$), stromal scores ($P < 0.001$), and ESTIMATE scores ($P < 0.001$) compared to those with low P3H1 expression (Fig. 6A). In contrast, the ESTIMATE algorithm showed that high P3H1 expression groups had lower tumor purity than low P3H1

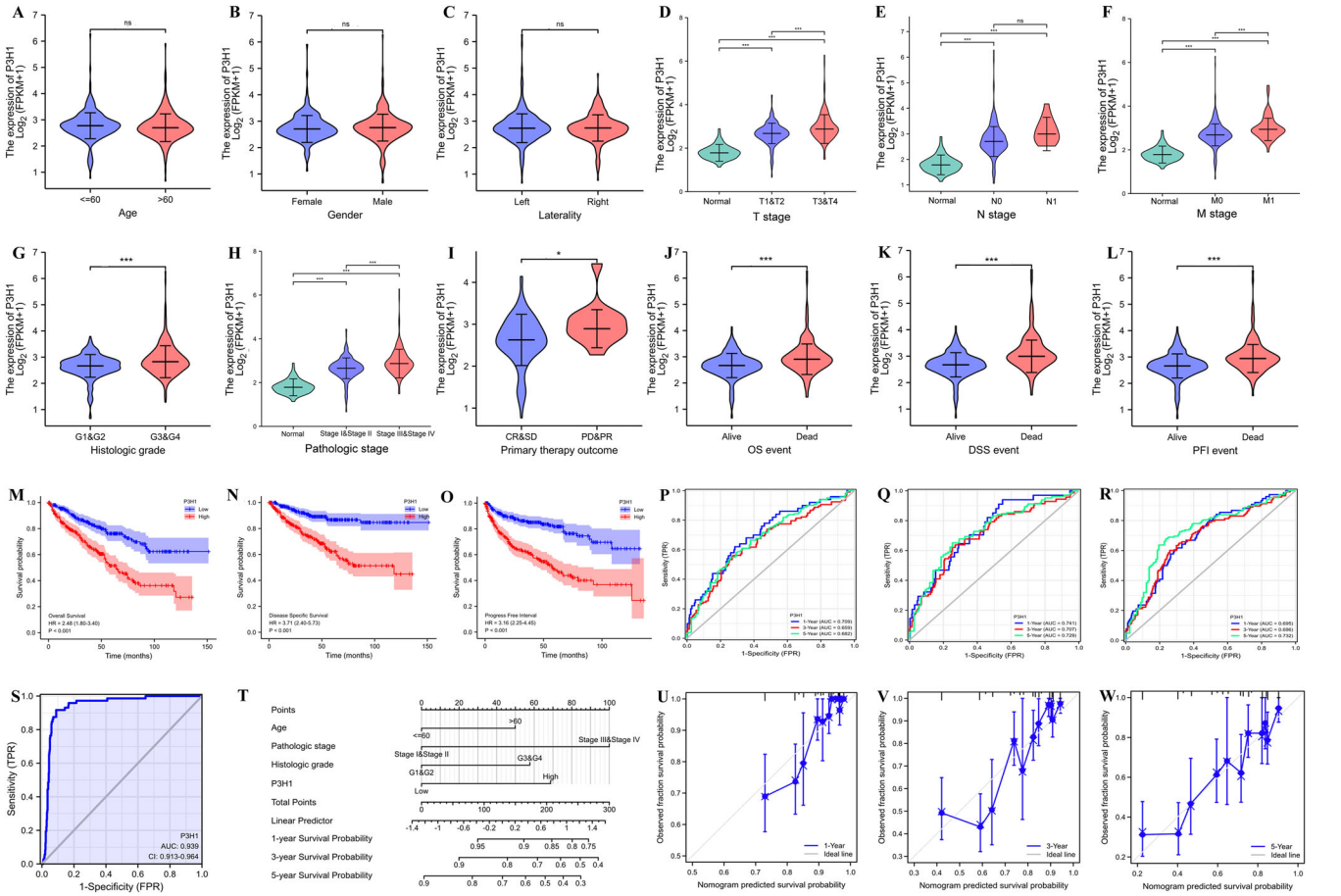

Fig. 4 | P3H1 expression levels correlate with multiple clinicopathological characteristics of ccRCC patients. **A**–**H** The correlation analysis between P3H1 expression levels and **A** age, **B** gender, **C** laterality, **D** T stage, **E** N stage, **F** M stage, **G** histologic grade, **H** pathological stage, **I** primary therapy outcome, **J** OS event, **K** DSS event and **L** PFI event of ccRCC patients. Kaplan-Meier, ROC analysis, nomogram and Calibration plot of P3H1. The Kaplan-Meier plotter analysis shows the differences in **M** overall survival, **N** disease-specific survival, and **O** progression-free interval of ccRCC patients with high- and low-P3H1 expression levels. ROC curve in **P** overall survival, **Q** disease-specific survival, and **R** progression-free interval of ccRCC patients with time dependence. **S** ROC curve showed that P3H1 had an AUC value of 0.939 to discriminate ccRCC tissues from healthy controls. **T** Nomogram for predicting the probability of 1-, 3-, and 5-year OS for ccRCC patients. **U**–**W** Calibration plot of the nomogram for predicting the OS likelihood of 1-, 3-, and 5-year OS for ccRCC patients. (ns: no significance; $^{*}P < 0.05$, $^{**}P < 0.01$, $^{***}P < 0.001$).

expression group (Fig. 6B). The thermogram of the immune function indicated that the high P3H1 expression group had significantly higher levels of cytolytic activity, inflammation-promoting, T-cell co-stimulation, and parainflammation (Fig. 6C). The EPIC algorithm revealed that the high P3H1 expression group had significantly higher levels of B cells, CAFs, and macrophages, while levels of CD4 + T cells, CD8 + T cells, and endothelial cells were not significantly different between the two groups (Fig. 6E). In contrast, the TIMER algorithm showed that the high-P3H1 expression group had increased levels of CD4 + T cells, neutrophils, and dendritic cells, with no significant difference in CD8 + T cells and macrophages compared to the low P3H1 expression group (Fig. 6D). The abundance of 22 immune cells in tumor tissues of ccRCC patients was evaluated using the CIBERSORT algorithm (Fig. 6F, G). The expression of four immune cells (Tregs, T cells CD4 memory activated, macrophages M0, and plasma cells) showed significant positive correlations with P3H1 expression in ccRCC. Conversely, the abundance of T cells gamma delta, monocytes, mast cells resting, macrophages M1, dendritic cells, and eosinophils was significantly negatively associated with P3H1 expression in ccRCC, as depicted in Fig. 6H and I. We found B cells showed significant differences between high and low P3H1 expression groups in the TIMER and EPIC algorithms (Fig. 6D, E), but no significant difference in CIBERSORT (Fig. 6F, G). CD8 + T cells did not show differences between the high and low P3H1 expression groups across the three immune algorithms (Fig. 6D–G). CD4 + T cells were enriched significantly in the high P3H1 expression group according to the TIMER algorithm (Fig. 6D), but there was no significant difference between the CIBERSORT and EPIC algorithms (Fig. 6E–G). Macrophages were significantly enriched in the high P3H1 expression group in the CIBERSORT and EPIC algorithms (Fig. 6E–G), while no significant difference was observed in the TIMER algorithm (Fig. 6D–G). Neutrophils were enriched significantly in the high P3H1 expression group according to the TIMER algorithm (Fig. 6D), but no significant difference was observed in the CIBERSORT algorithm (Fig. 6F, G). Correlation analysis using the CIBERSORT and ssGSEA algorithms showed that Tregs and macrophages were significantly positively correlated with P3H1 expression, while eosinophils were significantly negatively correlated with P3H1 expression (Fig. 6H, I). The CIBERSORT algorithm revealed a significant negative correlation between dendritic cells (DCs) and P3H1 expression, whereas the ssGSEA algorithm showed a significant positive correlation between DCs and P3H1 expression (Fig. 6H, I).

Exploration of the association between P3H1 and immunoinhibitors, immunostimulators, chemokines and chemokine receptors

Based on the TISIDB database, we further assessed the relationship between P3H1 expression and immunoinhibitors, immunostimulators, chemokines, and chemokine receptors. Figure 7A–D depicts the association between

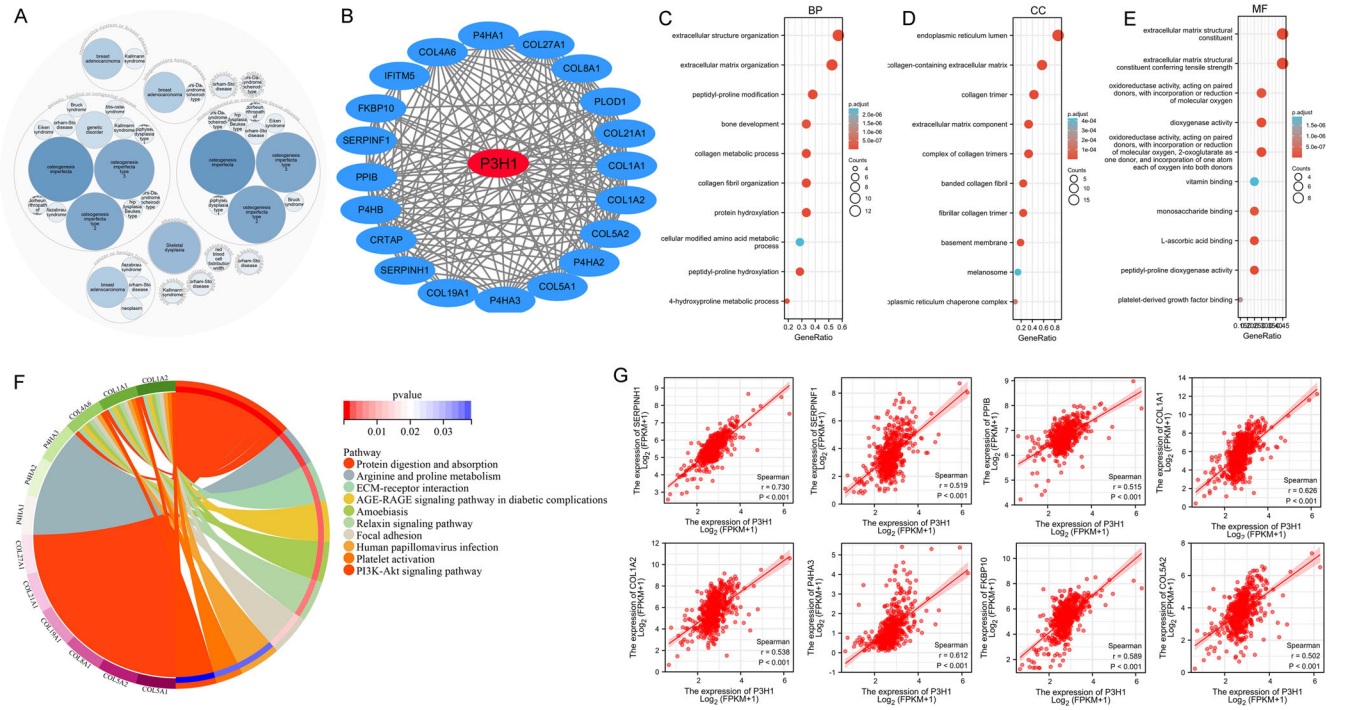

Fig. 5 | PPI network and functional enrichment analysis. A P3H1-associated diseases obtained by OPEN TARGET platform. **B** P3H1 and its co-expressed gene PPI network. BP **C**, CC **D**, MF **E**, KEGG **F** enrichment analysis of P3H1 and its 20 co-expressed genes. **G** Correlation analysis of P3H1 expression with co-expressed genes in ccRCC. BP Biological Process, CC Celluar Components, MF Molecular Functtion, KEGG Kyoto Encylopedia of Genes and Genomes, ccRCC clear cell renal cell carcinoma.

P3H1 expression and the abundance of immunoinhibitors and immunostimulators. Among the immunoinhibitors, the top three were CD274 (rho = -0.413, $P < 2.2e-16$), LGALS9 (rho = 0.438, $P < 2.2e-16$), and TGFB1 (rho = 0.545, $P < 2.2e-16$) (Fig. 7B). Among the immunostimulators, the top three were CD276 (rho = 0.609, $P < 2.2e-16$), CXCR4 (rho = 0.432, $P < 2.2e-16$), and IL6 (rho = 0.457, $P < 2.2e-16$) (Fig. 7D). The infiltration of immune cells into tumors depends on chemokines and chemokine receptors. The relationship between P3H1 expression and abundance of chemokines and chemokine receptors is shown in Fig. 7E–H. Among the chemokines, the top three were CCL11 (rho = 0.344, $P = 3.64e-16$), CCL26 (rho = 0.511, $P < 2.2e-16$), and CXCL5 (rho = 0.403, $P < 2.2e-16$) (Fig. 7F). Among the chemokines, the top three were CCR10 (rho = 0.409, $P < 2.2e-16$), CXCR4 (rho = 0.432, $P < 2.2e-16$), and CXCR5 (rho = 0.366, $P < 2.2e-16$) (Fig. 7H). These results suggest that P3H1 significantly correlates with various molecules involved in immunoinhibition, immunostimulation, chemokines, and chemokine receptors, indicating it may regulate these factors and impact the progression of ccRCC.

P3H1 expression level in immune cells

We evaluated P3H1 expression in immune cells using the HPA database, focusing on its specific expression in immune-infiltrating cells. P3H1 was primarily expressed in plasma blasts and memory Treg cells, as shown in the Monaco and Schmiedel datasets (Supplemental Fig. 2A, B). To explore the expression of P3H1 at the single-cell level, we carried out a single-cell analysis based on the TISCH database. We obtained five scRNA-seq datasets of ccRCC (GSE111360, GSE121636, GSE145281, GSE159115, GSE171360). Figure 8A illustrates the distribution of P3H1 expression across these datasets. In the GSE111360 dataset, which included 23,130 cells from two patients with primary ccRCC, P3H1 was predominantly expressed in fibroblasts and Tprolif cells (Fig. 8B). The GSE121636 dataset, comprising 33,441 cells from three patients with primary ccRCC, showed predominant expression of P3H1 in Tprolif cells (Fig. 8C). The GSE145281 dataset, encompassing 44,220 cells from tissues of four patients with metastatic ccRCC following immunotherapy (PD-L1), revealed significant differential expression of P3H1, particularly in plasma and Tprolif cells (Fig. 8D). The GSE159115 dataset, comprising 27,669 cells from tissues of eight patients with primary ccRCC, showed predominant expression of P3H1 in endothelial cells and pericytes (Fig. 8E). The GSE171360 dataset, containing 11,427 cells from tissues of two patients with primary ccRCC, demonstrated predominant expression of P3H1 in fibroblasts and endothelial cells (Fig. 8F). These results indicate that after PD-L1 treatment, ccRCC patients have higher plasma cell expression compared to untreated renal cancer patients. Additionally, after immunotherapy, the expression levels of immune cells in the tumor tissues of ccRCC patients are lower than those in untreated patients.

Predictive evaluation of P3H1 levels in ccRCC based on immune cells

Our findings suggest a potential mechanism for the influence of P3H1 expression on the prognosis of ccRCC patients through immune infiltration. To investigate this hypothesis, we analyzed whether P3H1 expression influences the prognosis of ccRCC patients in different immune cell subgroups. The Kaplan-Meier plotter unraveled a significant relationship between elevated P3H1 expression and poor prognosis in multiple enriched immune cell subgroups, including basophils ($P = 2.2e-08$), B cells ($P = 2.3e-05$), CD4+ memory T cells ($P = 7.2e-07$), CD8 + T cells ($P = 1.3e-06$), eosinophils ($P = 1.5e-05$), macrophages ($P = 5.3e-09$), mesenchymal stem cells ($P = 0.012$), regulatory T cells ($P = 3.4e-05$), Type 1 T helper cells ($P = 0.0053$), and Type 2 T helper cells ($P = 0.019$) (Supplemental Fig. 3). In parallel, elevated P3H1 expression in various immune cell subgroups was associated with poor prognosis, including basophils ($P = 3.5e-06$), B cells ($P = 1.9e-10$), CD4+ memory T cells ($P = 9.2e-07$), CD8 + T cells ($P = 7.2e-07$), eosinophils ($P = 1.9e-07$), macrophages ($P = 2.4e-05$), mesenchymal stem cells ($P = 4.1e-08$), natural killer T cells ($P = 7.8e-09$), regulatory T cells ($P = 7.6e-07$), Type 1 T helper cells ($P = 5.6e-09$), and Type 2 T helper cells ($P = 2.9e-10$) (Supplemental Fig. 3). However, there was no significant difference in survival between high and low P3H1 expression

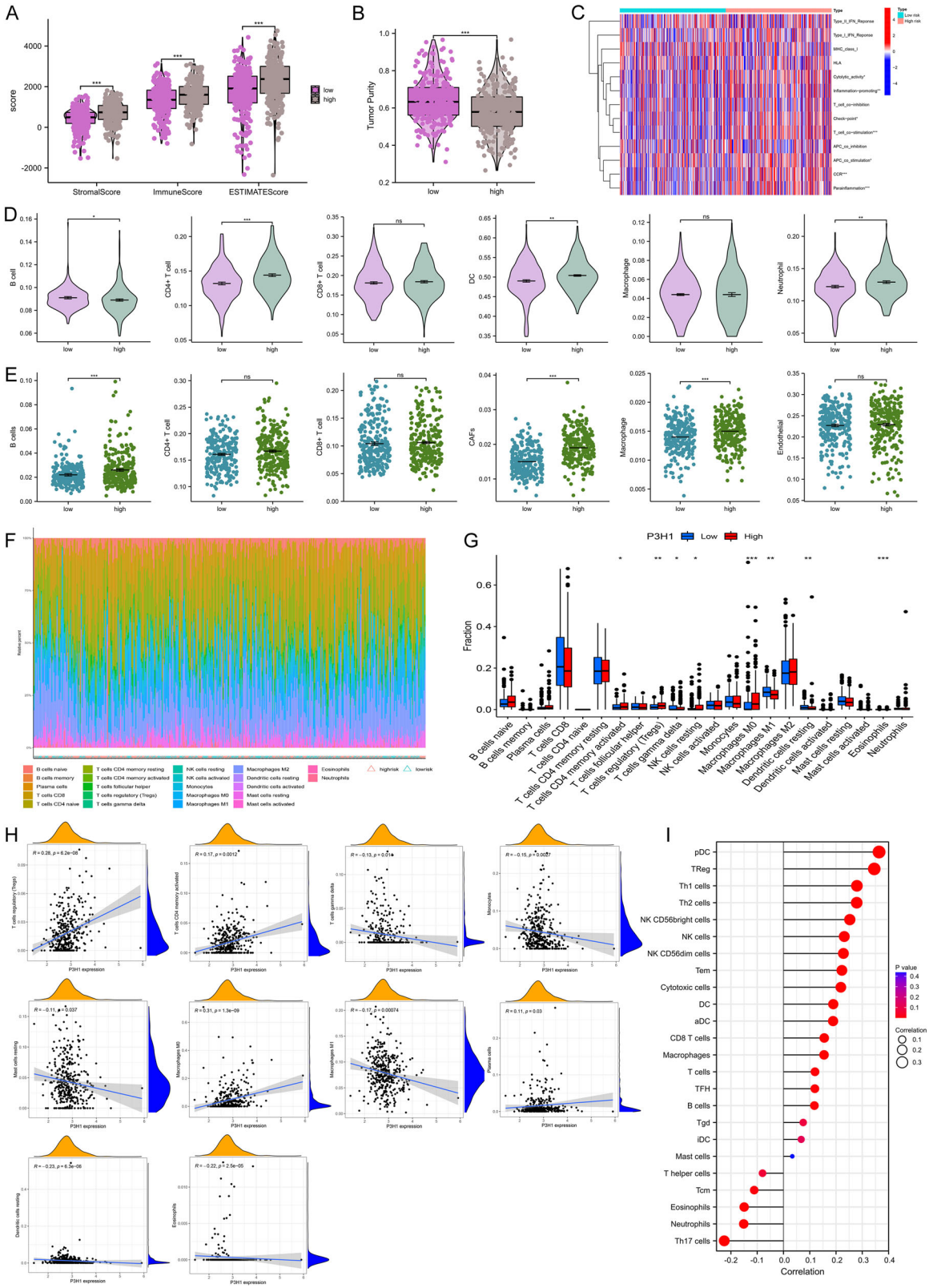

Fig. 6 | Immune infiltration analysis. A, **B** Stomal score, immune score, ESTIMATE score and tumor purity calculated by ESTIMATE algorithm. **C** Heat map of immune function. The abundance of immune filtrating cells was evaluated by the TIMER **D** and EPIC **E** algorithm. **F**, **G** The CIBERSORT algorithm was used to map 22 kinds of immune cells in tumor tissues of ccRCC patients. Correlation of P3H1 expression with immune infiltration level by the CIBERSORT **H** and ssGSEA algorithm **I**.

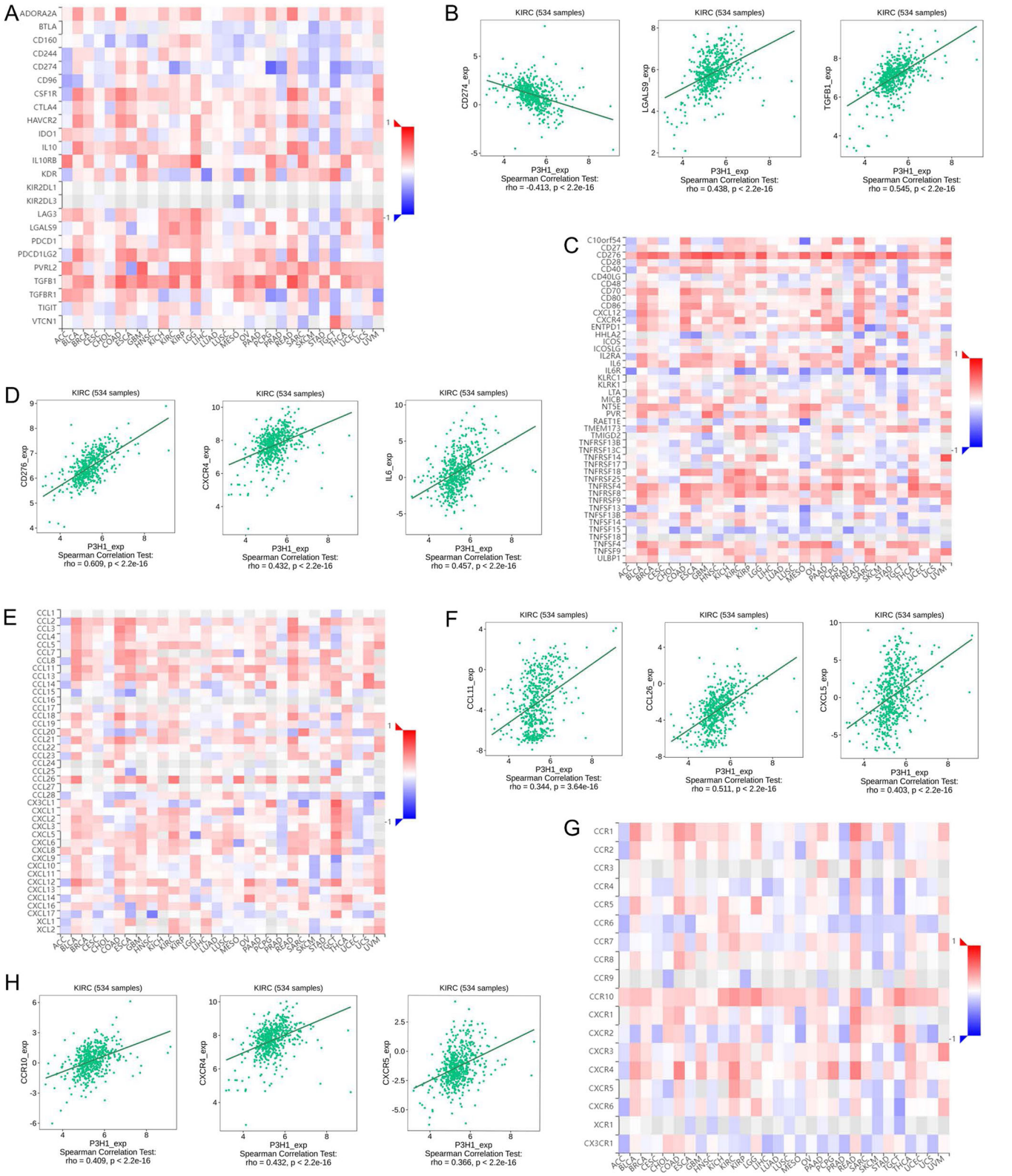

Fig. 7 | Associations of the P3H1 expression level with immunoinhibitors, immunostimulators, chemokines and chemokine receptors in ccRCC. Heatmaps for correlation analysis of the P3H1 expression level with immunoinhibitors (**A**), immunostimulators (**C**), chemokines (**E**) and chemokine receptors (**G**) in ccRCC. The top 3 immunoinhibitors (**B**), immunostimulators (**D**), chemokines (**F**), and receptors (**H**) associated with the expression of P3H1 in ccRCC.

groups in enriched natural killer T cells ($P = 0.13$) (Supplemental Fig. 3C). These results indicate that the impact of elevated P3H1 expression on the prognosis of ccRCC patients is partially mediated by immune infiltration.

Establishment of ceRNA co-expression network and related survival analysis

The P3H1-miRNA interaction data were obtained from the starBase database and analyzed using the R package. Based on a co-expressed and

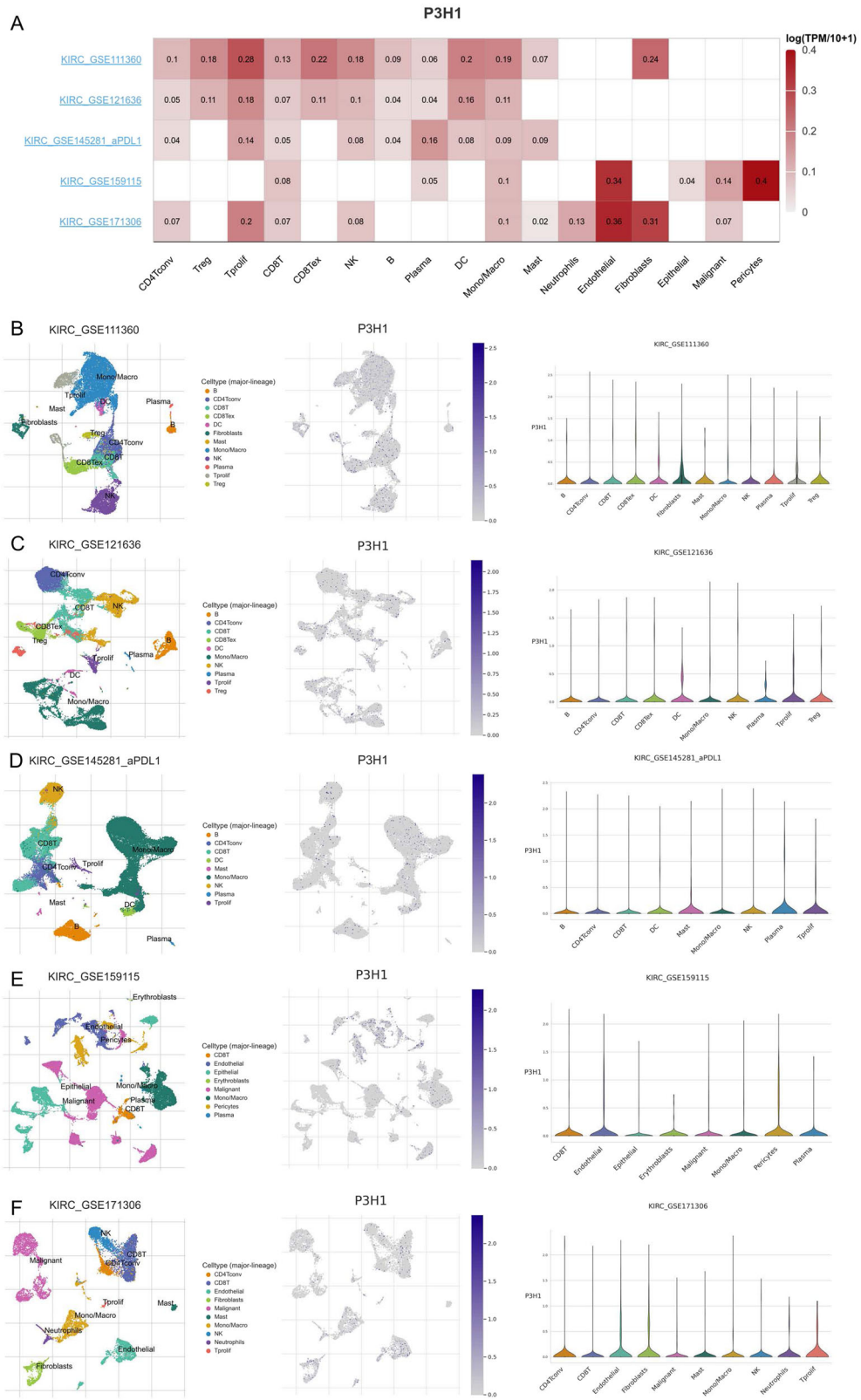

Fig. 8 | Single-cell analysis of the P3H1 and TME in ccRCC. A The expression levels of P3H1 in the TME-related cells of ccRCC in 5 independent scRNA-seq datasets; **B–F** Violin plots and UMAP plots of P3H1 and immune cell infiltration in GSE111360 (**B**), GSE121636 (**C**), GSE145281 (**D**), GSE159115 (**E**), GSE171360 (**F**).

negative correlation with P3H1 ($R < -0.2$; $P < 0.001$; Fig. 9), three groups of miRNAs were identified for subsequent screening of potential targets and pathways. Among these, two groups of miRNAs were observed differentially expressed between the normal and tumor groups ($P < 0.001$; Fig. 9A, C), and the above-mentioned miRNA-related prognosis survival curve analysis revealed that the high-expression group had a better survival rate compared to the low-expression group ($P < 0.01$; Fig. 9A, C).

Subsequently, we obtained lncRNA data that interacted with miR-10a-5p and miR-660-5p from the starBase database and performed a screening

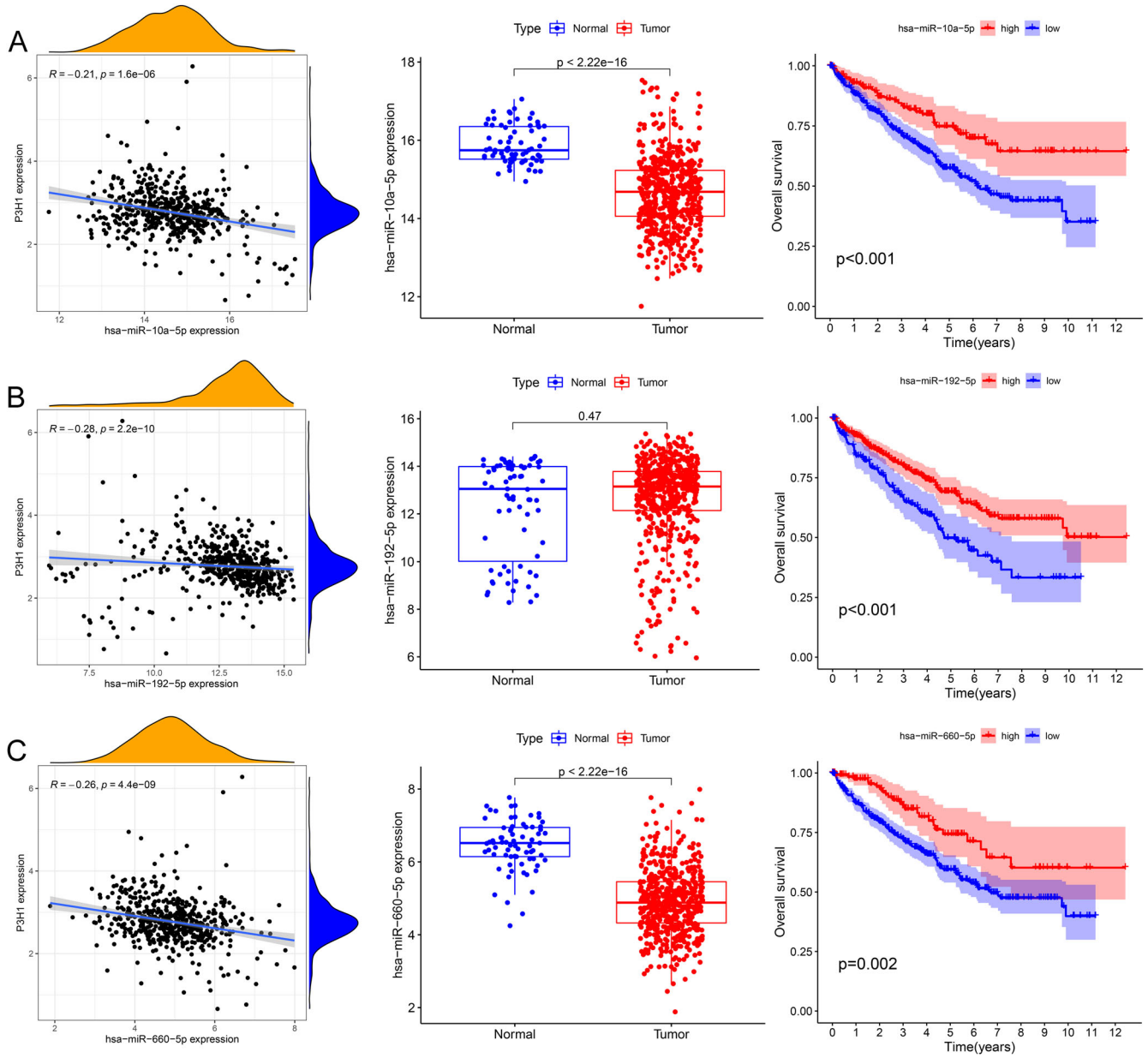

Fig. 9 | Correlation, difference, and survival curve analyses between P3H1 and 3 miRNAs. A miR-10a-5p; **B** miR-192-5p; **C** miR-660-5p.

process based on correlation coefficients (value > 0.1), survival curves, and differential expression between normal and tumor groups ($P < 0.01$). According to the screening results, we further selected lncRNAs that showed a positive correlation with P3H1, with a correlation coefficient value greater than 0.1 and a P value less than 0.01. Finally, the miR-10a-5p-related lncRNA (SNHG3) and the miR-660-5p-related lncRNA (GAS5) were identified (Fig. 10A, B). These results were used to construct a ceRNA mechanism diagram for P3H1, as shown in Fig. 10C. The ceRNA regulatory network revealed potential mechanisms of P3H1 in ccRCC, yet further experiments are needed to validate this regulatory network. This inquiry seeks to uncover novel regulatory mechanisms underlying P3H1's role in cancer biology and lays the groundwork for future translational studies aimed at developing personalized treatment strategies and prognostic biomarkers for ccRCC patients.

The relationship between immune checkpoint and P3H1 in ccRCC

Immune checkpoints are negative regulators of effector functions, proliferation, and T-cell activation. ICB has been explored as a potential approach to activate antitumor immunity against tumors. Hence, we evaluated the expression of seven immune checkpoint genes, namely PDCD1 (PD-1), CD274 (PD-L1), CTLA4, PDCD1LG2 (PD-L2), TIGIT, HAVCR2 (TIM-3), and LAG3, which have previously been reported as targets of ICB. The relationship between P3H1 expression and the expression of immune checkpoint genes was analyzed using the TIMER and TCGA databases. Spearman correlation analysis showed that the expression of P3H1 was significantly correlated with six immune markers (PDCD1, CTLA4, CD274, TIGIT, HAVCR2, and LAG3) ($|cor| > 0.1$ and $P < 0.05$) (Fig. 11C, D). Consistent results were also obtained from the analysis of the TIMER and GEPIA datasets (Fig. 11A, B). In conclusion, our study highlights that P3H1 expression correlates positively with key immune checkpoint genes, suggesting its potential role in modulating antitumor immune responses.

We then analyzed transcriptome sequencing data from 181 kidney cancer patients treated with nivolumab in the CM-025 cohort by Braun et al. to assess the effect of P3H1 on ICB in this group (Fig. 11E–H). The comprehensive analysis of the study cohort ($N = 181$) revealed a significant positive correlation between P3H1 and HAVCR2 (Fig. 11E). Further

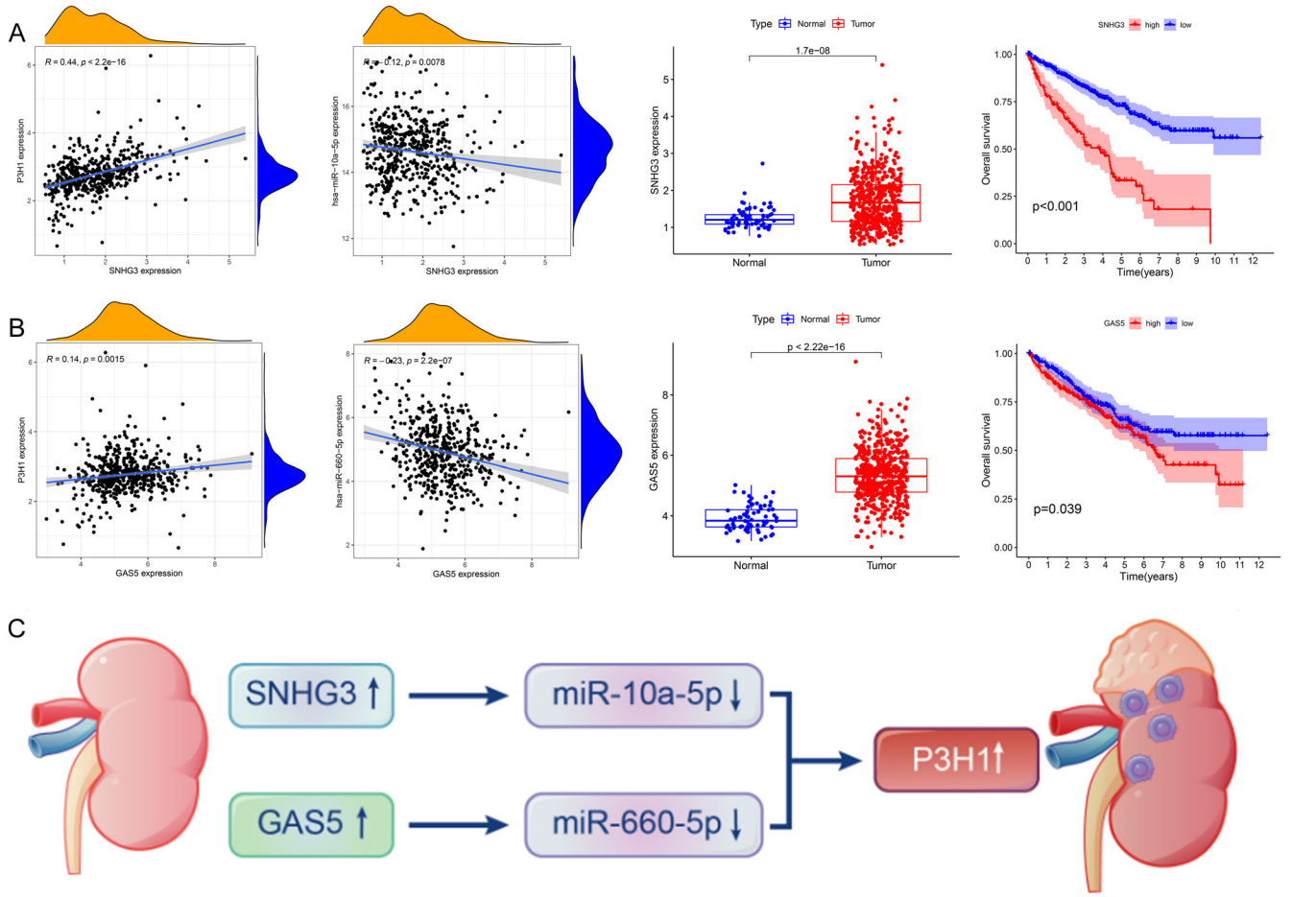

Fig. 10 | Construct a ceRNA regulatory network for P3H1. A Correlation, difference, and survival curve analyses between miR-10a-5p-P3H1-related lncRNA and miRNA and P3H1, respectively. **B** Correlation, difference, and survival curve analyses between miR-660-5p-P3H1-related lncRNA and miRNA and P3H1, respectively. **C** The model of P3H1-related ceRNA in the carcinogenesis of ccRCC.

investigation of progressive disease (PD) patients ($N = 69$) following treatment uncovered a robust positive relationship between P3H1 and HAVCR2, a correlation not evident with other immune checkpoints (Fig. 11F). Conversely, in the case of patients with stable disease (SD) post-treatment ($N = 64$), no significant associations were observed between P3H1 and any immune checkpoints (Fig. 11G). Lastly, in patients demonstrating partial response (PR) to treatment ($N = 13$), a notable negative correlation was identified between P3H1 and CTLA4, while no similar relationships were detected with other immune checkpoints (Fig. 11H). These findings further demonstrate that P3H1 plays an essential role in promoting tumor-immune evasion in the ccRCC microenvironment. These findings underscore the potential of P3H1 as a biomarker for predicting responses to immune checkpoint blockade in ccRCC patients treated with NIVOLUMAB.

Drug sensitivity evaluation

We examined the relationship between P3H1 and the sensitivity of ccRCC patients to several drugs commonly used in clinical treatment. The drugs included axitinib, sorafenib, pazopanib, sunitinib, gefitinib, and lapatinib. Our results indicated that patients with low P3H1 expression were generally more susceptible to most drugs compared to those with high P3H1 expression ($P < 0.001$; Supplemental Fig. 4). In conclusion, our analysis revealed that low P3H1 expression in ccRCC patients is associated with increased sensitivity to a range of commonly used drugs in clinical treatment. Particularly noteworthy, patients with high P3H1 expression demonstrated heightened susceptibility to gefitinib and lapatinib ($P < 0.001$; Supplemental Fig. 4), suggesting these drugs could be beneficial options for treating ccRCC patients with elevated P3H1 levels.

Discussion

ccRCC is a common type of urinary system tumor characterized by high levels of tumor-infiltrating immune cells and aggressive behavior[38]. Conventional radiotherapy and chemotherapies have exhibited limited effectiveness in treating advanced ccRCC, and therefore targeted therapy and immunotherapy are the primary treatment options[39,40]. Nevertheless, the long-term efficacy of these treatments in treating advanced KIRC remains suboptimal due to the absence of precise targets.

P3H1 plays a crucial role in collagen synthesis and folding, which are essential for maintaining structural integrity in tissues. Emerging evidence suggests that P3H1 may have significant implications in tumorigenesis and tumor progression across various cancers. Further research is needed to fully elucidate the molecular mechanisms through which P3H1 influences ccRCC biology, potentially offering new insights into diagnostic and therapeutic strategies for ccRCC treatment.

In this research, we examined the P3H1 expression in ccRCC tumor tissues and adjacent normal tissues and found that P3H1 expression was elevated significantly in ccRCC. These results were further certified by both immunohistochemistry assay and qRT-PCR analysis. Elevated expression of P3H1 was associated with higher T and M stages as well as higher histologic and pathologic stages in a positive way. The Kaplan Meier-Plotter database analysis revealed that high expression levels of P3H1 in a variety of immune cell cohorts of ccRCC were associated with a worse prognosis. The results of the Kaplan-Meier curves and univariate analysis have demonstrated that elevated expression of P3H1 was correlated with short OS, DSS, and PFI. Time-dependent ROC curve analysis suggested that P3H1 might be a potentially valuable diagnostic biomarker for distinguishing between

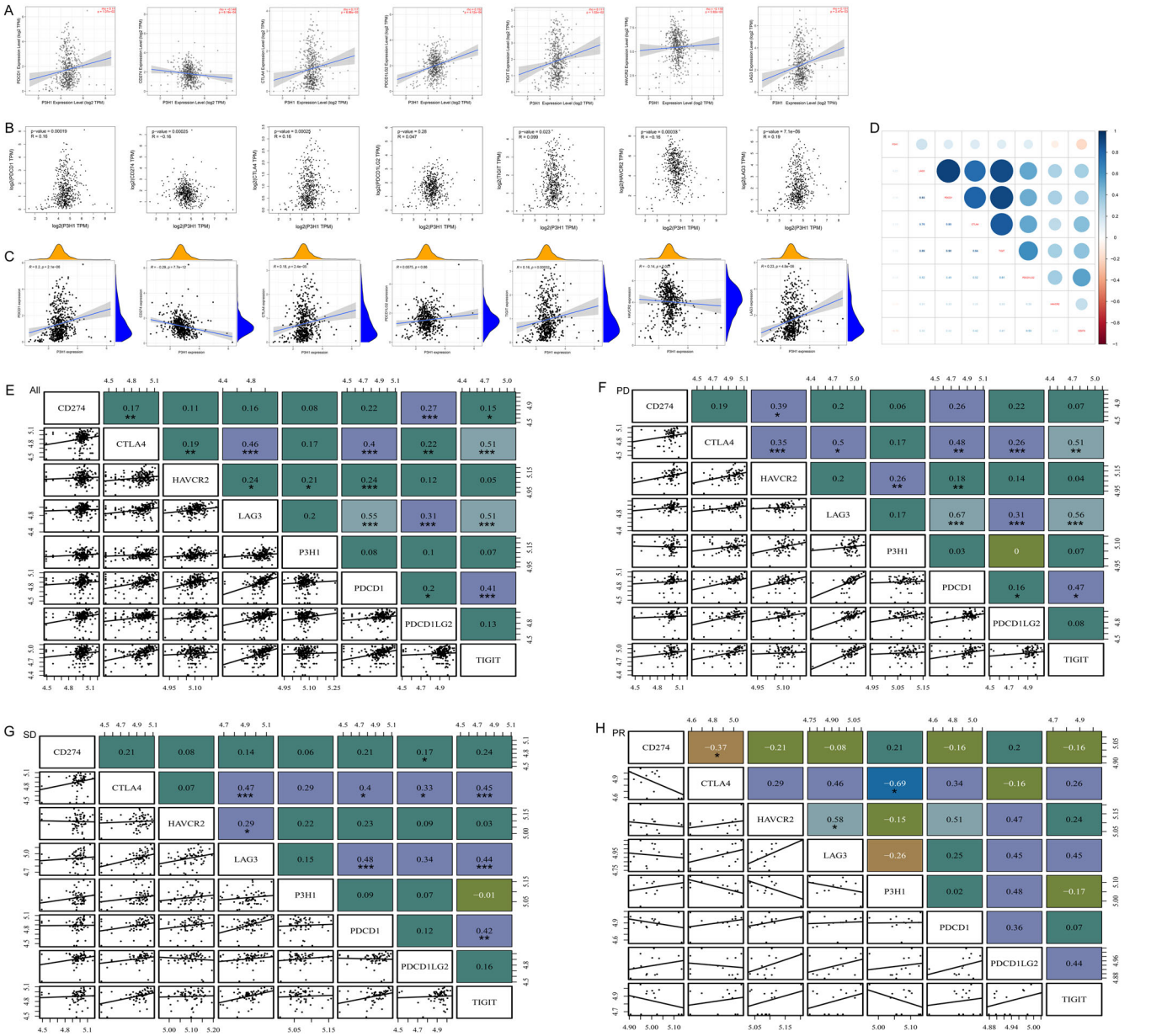

Fig. 11 | The relationship between P3H1 expression and immune checkpoint genes in ccRCC. The expression correlation of P3H1 with PDCD1 (PD-1), CD274 (PD-L1), CTLA4, PDCD1LG2 (PD-L2), TIGIT, HAVCR2 (TIM-3), and LAG3 in ccRCC was investigated by TIMER (**A**), GEPIA (**B**), and the spearman correlation analysis of TCGA data (**C**). **D** Correlation heat map between P3H1 and immune checkpoints. **E** Association of P3H1 with immune checkpoint genes in 181 kidney cancer patients treated with NIVOLUMAB in the CheckMate 025 (CM-025) cohort. Association of P3H1 with immune checkpoint genes in PD (**F**), SD (**G**), and PR (**H**) after NIVOLUMAB treatment in the CheckMate 025 (CM-025) cohort.

ccRCC and normal tissues. These findings imply that P3H1 might exert a key role in the progression of ccRCC.

Previous studies have shown that ccRCC has a high level of immune infiltration[41–43]. Nonetheless, the correlation analysis of P3H1 expression and immune cell infiltration in ccRCC has not been reported. Our study has shown that multiple immune cells infiltrate tumors. We observed a positive correlation between P3H1 expression and abundance of Tregs, T cells CD4 memory activated, macrophages M0, and plasma cells. Tregs are a subset of T lymphocytes that suppress anti-tumor responses, leading to tumor immune escape[44,45]. Previous studies also linked the proportion of macrophages and Tregs in RCC patients with poor prognosis[46,47]. These results suggest that elevated expression of P3H1 may partly affect the prognosis of ccRCC patients through its impact on immune infiltration.

Additionally, we investigated the relationship between P3H1 and immune checkpoints in both the untreated TCGA-KIRC cohort without prior immunotherapy and the NIVOLUMAB-treated CM-025 cohort. In the TCGA-KIRC cohort, P3H1 expression exhibited positive correlations with several immune checkpoints, including PDCD1, CTLA4, PDCD1LG2, TIGIT, and LAG3, implying its potential involvement in immune evasion during ccRCC carcinogenesis. Subsequent analysis of the NIVOLUMAB-treated cohort showed a significant positive correlation between P3H1 and HAVCR2 in patients with PD, with no significant correlations observed in SD patients, while notably, P3H1 exhibited a significant negative correlation with CTLA4 in patients showing PR. These findings underscore P3H1's potential as a biomarker for predicting responses to immune checkpoint blockade in ccRCC patients treated with NIVOLUMAB.

The ceRNA regulatory network has been demonstrated to play a role in the development and progression of cancers[48]. These networks involve ncRNAs that regulate gene expression by competing for binding sites with other RNAs[49–51]. In the current study, we employed bioinformatics analysis

of gene chip data to construct a comprehensive ceRNA network for P3H1 deletion, which is involved in regulating ccRCC proliferation. We identified several ncRNAs, including miR-10a-5p, miR-660-5p, GAS5, and SNHG3, which have been previously investigated in cancer or specifically in KIRC[52–55]. Notably, miR-10a-5p and miR-660-5p, known tumor suppressors, are significantly downregulated in ccRCC, with their low expression correlating with increased cell migration, invasion, and proliferation[55,56]. This research aims to uncover novel regulatory mechanisms of P3H1 in cancer biology and to lay the groundwork for future studies on personalized treatment strategies and prognostic biomarkers for ccRCC patients.

Our study has several limitations. Firstly, the findings are based on bioinformatics analysis and need validation through further experimental research. While the bioinformatics analysis provided valuable insights into the relationship between P3H1 expression and ccRCC prognosis, immune infiltration, immune checkpoints, and drug sensitivity, the results should be interpreted with caution until confirmed by experimental studies. Additionally, this study focused solely on P3H1 expression in ccRCC, and it remains unclear whether these findings are generalizable to other types of cancer. Further research is needed to investigate the role of P3H1 in various cancer types and to validate our findings in experimental models.

This study employs a multidimensional approach integrating vitro assays and multi-omics bioinformatics analyses to investigate P3H1's impact on ccRCC prognosis, immune modulation, immune checkpoints, ceRNA regulatory network, drug sensitivity, and therapeutic responses, aiming to uncover new insights into its therapeutic potential and inform future clinical strategies.

Data availability

All data are obtained in the article.

Received: 27 February 2024; Accepted: 28 October 2024;
Published online: 08 November 2024

References

1. Siegel, R. L., Giaquinto, A. N. & Jemal, A. Cancer statistics, 2024. *CA: a cancer J. Clin.* **74**, 12–49 (2024).
2. Ding, G. et al. Wiskott-Aldrich syndrome gene as a prognostic biomarker correlated with immune infiltrates in clear cell renal cell carcinoma. *Front. Immunol.* **14**, 1102824 (2023).
3. Hutson, T. E. & Figlin, R. A. Renal cell cancer. *Cancer J. (Sudbury, Mass)* **13**, 282–286 (2007).
4. Hsieh, J. J. et al. Chromosome 3p loss-orchestrated VHL, HIF, and epigenetic deregulation in clear cell renal cell carcinoma. *J. Clin. Oncol. : Off. J. Am. Soc. Clin. Oncol.* **36**, Jco2018792549 (2018).
5. Topalian, S. L. et al. Five-year survival and correlates among patients with advanced melanoma, renal cell carcinoma, or non-small cell lung cancer treated with nivolumab. *JAMA Oncol.* **5**, 1411–1420 (2019).
6. Ding, G. et al. A novel prognostic predictor of immune microenvironment and therapeutic response in clear cell renal cell carcinoma based on angiogenesis-immune-related gene signature. *Heliyon* **10**, e23503 (2024).
7. Li, Q. K., Pavlovich, C. P., Zhang, H., Kinsinger, C. R. & Chan, D. W. Challenges and opportunities in the proteomic characterization of clear cell renal cell carcinoma (ccRCC): A critical step towards the personalized care of renal cancers. *Semin. cancer Biol.* **55**, 8–15 (2019).
8. Majer, W., Kluzek, K., Bluyssen, H. & Wesoły, J. Potential approaches and recent advances in biomarker discovery in clear-cell renal cell carcinoma. *J. Cancer* **6**, 1105–1113 (2015).
9. Kaul, S. C., Sugihara, T., Yoshida, A., Nomura, H. & Wadhwa, R. Gros1, a potential growth suppressor on chromosome 1: its identity to basement membrane-associated proteoglycan, leprecan. *Oncogene* **19**, 3576–3583 (2000).
10. Vranka, J. A., Sakai, L. Y. & Bächinger, H. P. Prolyl 3-hydroxylase 1, enzyme characterization and identification of a novel family of enzymes. *J. Biol. Chem.* **279**, 23615–23621 (2004).
11. Marini, J. C., Cabral, W. A., Barnes, A. M. & Chang, W. Components of the collagen prolyl 3-hydroxylation complex are crucial for normal bone development. *Cell cycle (Georget., Tex.)* **6**, 1675–1681 (2007).
12. Wassenhove-McCarthy, D. J. & McCarthy, K. J. Molecular characterization of a novel basement membrane-associated proteoglycan, leprecan. *J. Biol. Chem.* **274**, 25004–25017 (1999).
13. Huang, Z. et al. Upregulated LEPRE1 correlates with poor outcome and its knockdown attenuates cells proliferation, migration and invasion in osteosarcoma. *Anti-cancer drugs* **31**, 326–332 (2020).
14. Willumsen, N. et al. Serum biomarkers reflecting specific tumor tissue remodeling processes are valuable diagnostic tools for lung cancer. *Cancer Med.* **3**, 1136–1145 (2014).
15. Bager, C. L. et al. Collagen degradation products measured in serum can separate ovarian and breast cancer patients from healthy controls: A preliminary study. *Cancer Biomark. : Sect. A Dis. Markers* **15**, 783–788 (2015).
16. Kehlet, S. N. et al. Excessive collagen turnover products are released during colorectal cancer progression and elevated in serum from metastatic colorectal cancer patients. *Sci. Rep.* **6**, 30599 (2016).
17. Li Y, Wang T, Jiang F. Pan-cancer analysis of P3H1 and experimental validation in renal clear cell carcinoma. *Appl. Biochem. Biotechnol*. 2024.
18. Li, C. et al. The prognostic significance and potential mechanism of prolyl 3-hydroxylase 1 in hepatocellular carcinoma. *J. Oncol.* **2022**, 7854297 (2022).
19. Kopp, F. & Mendell, J. T. Functional classification and experimental dissection of long noncoding RNAs. *Cell* **172**, 393–407 (2018).
20. Lu, T. X. & Rothenberg, M. E. MicroRNA. *J. allergy Clin. Immunol.* **141**, 1202–1207 (2018).
21. Yang, C. et al. Competing endogenous RNA networks in human cancer: hypothesis, validation, and perspectives. *Oncotarget* **7**, 13479–13490 (2016).
22. Salmena, L., Poliseno, L., Tay, Y., Kats, L. & Pandolfi, P. P. A ceRNA hypothesis: the Rosetta Stone of a hidden RNA language? *Cell* **146**, 353–358 (2011).
23. Nejadi Orang, F. & Abdoli Shadbad, M. Competing endogenous RNA networks and ferroptosis in cancer: novel therapeutic targets. *Cell death Dis.* **15**, 357 (2024).
24. Uhlén, M. et al. Proteomics. Tissue-based map of the human proteome. *Sci. (N. Y., NY)* **347**, 1260419 (2015).
25. Braun, D. A. et al. Interplay of somatic alterations and immune infiltration modulates response to PD-1 blockade in advanced clear cell renal cell carcinoma. *Nat. Med.* **26**, 909–918 (2020).
26. Yoshihara, K. et al. Inferring tumour purity and stromal and immune cell admixture from expression data. *Nat. Commun.* **4**, 2612 (2013).
27. Li, T. et al. TIMER2.0 for analysis of tumor-infiltrating immune cells. *Nucleic Acids Res.* **48**, W509–w14 (2020).
28. Li, B. et al. Comprehensive analyses of tumor immunity: implications for cancer immunotherapy. *Genome Biol.* **17**, 174 (2016).
29. Racle J, de Jonge K, Baumgaertner P, Speiser DE, Gfeller D. Simultaneous enumeration of cancer and immune cell types from bulk tumor gene expression data. eLife. 6, e26476 (2017).
30. Newman, A. M. et al. Robust enumeration of cell subsets from tissue expression profiles. *Nat. methods* **12**, 453–457 (2015).
31. Tang, Z., Kang, B., Li, C., Chen, T. & Zhang, Z. GEPIA2: an enhanced web server for large-scale expression profiling and interactive analysis. *Nucleic Acids Res.* **47**, W556–w60 (2019).
32. Ru, B. et al. TISIDB: an integrated repository portal for tumor-immune system interactions. *Bioinforma. (Oxf., Engl.)* **35**, 4200–4202 (2019).
33. Han, Y. et al. TISCH2: expanded datasets and new tools for single-cell transcriptome analyses of the tumor microenvironment. *Nucleic Acids Res.* **51**, D1425–d31 (2023).

34. Szklarczyk, D. et al. The STRING database in 2023: protein-protein association networks and functional enrichment analyses for any sequenced genome of interest. *Nucleic acids Res.* **51**, D638–d46 (2023).
35. Yu, G., Wang, L. G., Han, Y. & He, Q. Y. clusterProfiler: an R package for comparing biological themes among gene clusters. *Omics : a J. Integr. Biol.* **16**, 284–287 (2012).
36. Li, J. H., Liu, S., Zhou, H., Qu, L. H. & Yang, J. H. starBase v2.0: decoding miRNA-ceRNA, miRNA-ncRNA and protein-RNA interaction networks from large-scale CLIP-Seq data. *Nucleic acids Res.* **42**, D92–D97 (2014).
37. Geeleher, P., Cox, N. & Huang, R. S. pRRophetic: an R package for prediction of clinical chemotherapeutic response from tumor gene expression levels. *PloS one* **9**, e107468 (2014).
38. Zhu, G. et al. Profiles of tumor-infiltrating immune cells in renal cell carcinoma and their clinical implications. *Oncol. Lett.* **18**, 5235–5242 (2019).
39. Pal, S. K. et al. CD70-targeted allogeneic CAR T-cell therapy for advanced clear cell renal cell carcinoma. *Cancer Discov.* **14**, 1176–1189 (2024).
40. Reustle, A. et al. Integrative-omics and HLA-ligandomics analysis to identify novel drug targets for ccRCC immunotherapy. *Genome Med.* **12**, 32 (2020).
41. Zhang Y, et al. Single-cell analyses of renal cell cancers reveal insights into tumor microenvironment, cell of origin, and therapy response. *Proc. Nat. Acad. Sci. USA*. 118, e2103240118 (2021).
42. Chevrier, S. et al. An immune atlas of clear cell renal cell carcinoma. *Cell* **169**, 736–749.e18 (2017).
43. Geissler, K. et al. Immune signature of tumor infiltrating immune cells in renal cancer. *Oncoimmunology* **4**, e985082 (2015).
44. Sakaguchi, S., Miyara, M., Costantino, C. M. & Hafler, D. A. FOXP3+ regulatory T cells in the human immune system. *Nat. Rev. Immunol.* **10**, 490–500 (2010).
45. Tanaka, A. & Sakaguchi, S. Regulatory T cells in cancer immunotherapy. *Cell Res.* **27**, 109–118 (2017).
46. Shang, B., Liu, Y., Jiang, S. J. & Liu, Y. Prognostic value of tumor-infiltrating FoxP3+ regulatory T cells in cancers: a systematic review and meta-analysis. *Sci. Rep.* **5**, 15179 (2015).
47. Cros, J. et al. Nestin expression on tumour vessels and tumour-infiltrating macrophages define a poor prognosis subgroup of pt1 clear cell renal cell carcinoma. *Virchows Arch. : Int. J. Pathol.* **469**, 331–337 (2016).
48. Su, X. et al. microRNAs and ceRNAs: RNA networks in pathogenesis of cancer. Chinese journal of cancer research. *Chung-kuo yen cheng yen chiu* **25**, 235–239 (2013).
49. Razavi, Z. S. et al. Gynecologic cancers and non-coding RNAs: Epigenetic regulators with emerging roles. *Crit. Rev. Oncol./Hematol.* **157**, 103192 (2021).
50. Ghafouri-Fard, S., Shoorei, H., Anamag, F. T. & Taheri, M. The role of non-coding RNAs in controlling cell cycle related proteins in cancer cells. *Front. Oncol.* **10**, 608975 (2020).
51. Lou, W., Ding, B., Wang, J. & Xu, Y. The Involvement of the hsa_circ_0088494-miR-876-3p-CTNNB1/CCND1 axis in carcinogenesis and progression of papillary thyroid carcinoma. *Front. Cell Dev. Biol.* **8**, 605940 (2020).
52. Yang, W. et al. Discovery and validation of the prognostic value of the lncRNAs encoding snoRNAs in patients with clear cell renal cell carcinoma. *Aging* **12**, 4424–4444 (2020).
53. Arai, T. et al. Regulation of spindle and kinetochore-associated protein 1 by antitumor miR-10a-5p in renal cell carcinoma. *Cancer Sci.* **108**, 2088–2101 (2017).
54. Li, J., Li, Y., He, X. & Zhao, Q. Gain of GAS5 reveals worse prognosis in kidney renal clear cell carcinoma and liver hepatocellular carcinoma from the Cancer Genome Atlas dataset. *Transl. cancer Res.* **10**, 223–232 (2021).
55. He, T. et al. miR-660-5p is associated with cell migration, invasion, proliferation and apoptosis in renal cell carcinoma. *Mol. Med. Rep.* **17**, 2051–2060 (2018).
56. Liu, R. J. et al. BAP1-related ceRNA (NEAT1/miR-10a-5p/SERPINE1) promotes proliferation and migration of kidney cancer cells. *Front. Oncol.* **12**, 852515 (2022).

Acknowledgements

This work was supported by the National Natural Science Foundation of China (Nos. 82370690, 82073131), Natural Science Foundation of Shandong Province (Nos. ZR2023MH241, ZR2021MH203), and Taishan Scholars Program of Shandong Province (Nos. tsqn201909199, tsqn202306403).

Author contributions

WJ, CY, DG, and WG designed this study. DG, WT, SF, CY, YS, LM, and TG performed writing, figures plotted, and data analysis. CY, WG, MJ, DG, and WJ critically reviewed the manuscript. All authors contributed to the article and approved the final version for submission.

Competing interests

The authors declare no competing interests.

Additional information

Supplementary information The online version contains supplementary material available at https://doi.org/10.1038/s41698-024-00748-x.

Correspondence and requests for materials should be addressed to Yuanshan Cui, Gang Wu or Jitao Wu.